PHILOSOPHICAL TRANSACTIONS OF THE ROYAL SOCIETY A MATHEMATICAL, PHYSICAL & ENGINEERING SCIENCES

Comparison of Series Expansion and Finite-Difference Computations of Internal Laminar Flow Separation

N. M. Bujurke, T. J. Pedley and O. R. Tutty

Phil. Trans. R. Soc. Lond. A 1996 **354**, 1751-1773
doi: 10.1098/rsta.1996.0077

Comparison of series expansion and finite-difference computations of internal laminar flow separation

By N. M. Bujurke[1], T. J. Pedley[2] and O. R. Tutty[3]

[1]*Department of Mathematics, Karnatak University, Dharwad 580003, India*
[2]*Department of Applied Mathematics and Theoretical Physics, University of Cambridge, Cambridge CB3 9EW, UK*
[3]*Department of Aero- and Astronautics, University of Southampton, Southampton SO17 1BJ, UK*

Contents

We present computed results for steady viscous flow in a two-dimensional channel with one plane wall and the other wall parallel far upstream but not parallel elsewhere. The particular example studied most fully is that of gradual exponential divergence. The main aim is to see whether a series expansion approach is as good as a finite difference method in computing flow separation in a diverging channel at moderately large values of the Reynolds number Re. It is assumed that the wall slope parameter ϵ is small but that ϵRe is not. The leading term of the series expansion is that given by lubrication theory, and the expansion proceeds in powers of ϵRe; two versions of the series are considered, one based on the boundary layer equations and one in which the leading effect of cross-stream pressure gradient is included. Convergence of the series is enhanced by the use of Padé approximants. Estimates are made of the position of the separation point, x_s, at various values of ϵRe $(= 1, 3, 5)$; the values of x_s on the two walls are somewhat different if the cross-stream pressure gradient is included. The results are compared with those of finite difference solutions of (*a*) the boundary layer equations and (*b*) the full Navier–Stokes equations. The boundary-layer and series-expansion results (with no cross-stream pressure gradient) agree extremely well, but to use the series method for more general wall geometries would be forbiddingly cumbersome, especially with cross-stream pressure gradient included.

Phil. Trans. R. Soc. Lond. A (1996) **354**, 1751–1773
Printed in Great Britain

The Navier–Stokes computations fail to provide a converged symmetric solution in which separation occurs at approximately the same value of x_s on each wall, but gives two converged solutions with the first separation point on one wall or the other. If too crude a convergence criterion had been used, a 'symmetric' solution would have been found. Such non-uniqueness is to be expected; the 'symmetric' flow (the only one achieveable by the series method) would presumably be unstable. None of the computed solutions predict that separation occurs as early as has been seen experimentally in a slightly different geometry.

1. Introduction

This paper is a contribution to the study of steady separated flow of an incompressible fluid in non-uniform, two-dimensional channels. It is well known that, if the cross-sectional area of such a channel increases gradually (but not too gradually) with distance downstream (x), the flow separates for values of the Reynolds number above a rather moderate critical value; moreover the separated flow is non-unique. Even when the geometry is symmetric, so that a symmetric solution to the equation of motion exists, the flow is normally asymmetric, clinging to one wall or another, the symmetric flow being unstable (Patterson 1934; Reneau *et al.* 1967; Ward-Smith 1980; Sobey & Drazin 1986; Durst *et al.* 1993). Borgas & Pedley (1990) showed analytically that this non-uniqueness occurs at large Reynolds number in channels that are sufficiently slowly varying for the flow to be governed by the boundary layer equations, in which there is neither a transverse pressure gradient nor longitudinal viscous diffusion. The channel is taken to be uniform for $x < 0$, with Poiseuille flow upstream, and after the expansion begins the flow consists of an inviscid core with thin viscous layers at the walls. In the similarity solutions obtained by these authors a supercritical pitchfork bifurcation takes place when the rate of expansion of channel width (equivalent to the magnitude of the adverse pressure gradient) is increased above a critical value.

The existence of asymmetric solutions of the boundary layer equations has not yet been confirmed by direct numerical integration: even in an asymmetric channel geometry, separation occurs symmetrically, i.e. at the same longitudinal location on each wall. The main aim of this paper is to investigate whether series methods (Van Dyke 1984) can be used to shed light on the internal separation process, particularly for an asymmetric geometry.

We take the slowly varying channel to be as depicted in figure 1, with rigid boundaries at $y = 0$ and $y = F(x)$, where $F(x) \to 1$ as $x \to -\infty$. The dimensionless coordinates are $(\epsilon^{-1}x, y)$ with corresponding velocity components $(u, \epsilon v)$, where the wall-slope parameter ϵ is taken to be very small. Far upstream there is Poiseuille flow, with $v = 0$ and

$$u = U_0(y) \equiv Gy(1-y), \tag{1.1}$$

where $G = 6$ to give unit dimensionless flow rate. The full governing equations are

$$u_x + v_y = 0, \tag{1.2}$$

$$\epsilon Re(uu_x + vu_y) = -p_x + u_{yy} + \epsilon^2 u_{xx}, \tag{1.3}$$

$$\epsilon^3 Re(uv_x + vv_y) = -p_y + \epsilon^2(v_{yy} + \epsilon^2 v_{xx}), \tag{1.4}$$

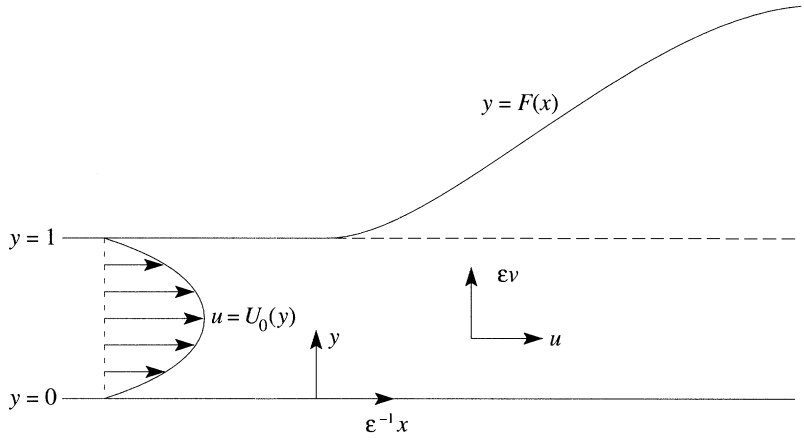

Figure 1. Sketch of asymmetric channel geometry, showing dimensionless coordinate system and velocity components. There is Poiseuille flow far upstream.

where p is the dimensionless pressure and Re the Reynolds number. The boundary conditions are that $u = v = 0$ on $y = 0$ and $y = F(x)$.

When ϵ^2 is neglected with respect to 1, these equations reduce to the boundary-layer equations, with (1.4) giving $p_y = 0$ and (1.3) becoming

$$\epsilon Re(uu_x + vu_y) = -p_x(x) + u_{yy}. \tag{1.5}$$

If ϵRe is also vanishingly small, the problem becomes one of lubrication theory, with

$$u = U_0[y/F(x)] \quad \text{and} \quad G = 6/F(x) \tag{1.6}$$

(so that $p_x = -12/F^3(x)$). The quantities ϵ^2 and ϵRe are independent parameters in (1.2)–(1.4), and the effect of inertia on the flow in a slowly varying channel can be analysed by keeping $\epsilon^2 \ll 1$ and solving (1.5) with (1.2). This can be done by finite-difference computations, as in § 3 below, or, for values of ϵRe that are not too large, by a series solution in powers of ϵRe, a procedure initiated by Blasius (1910). In fact, experience with series solutions of other problems (Van Dyke 1984) suggests that, if it is taken far and accurately enough, the series can be manipulated to give useful information at fairly *large* values of ϵRe. Such a procedure is attempted here, in § 2, with attention focused on predicting the value of x at which the flow first separates in a channel with

$$F(x) \equiv 1 + \beta g(x), \tag{1.7}$$

where β is an $O(1)$ constant (in the theory of Borgas & Pedley (1990), β was taken to be small, proportional to $(\epsilon Re)^{-1/3}$). We pay particular attention to the case

$$g(x) \equiv \mathrm{e}^x, \tag{1.8}$$

because the coefficients in the series expansion are particularly simple in that case. This form for $g(x)$ also corresponds fairly closely to the channel used in the experiments of Patterson (1934, 1935), who was attempting to test Blasius's (1910) theory. (In fact Patterson used a symmetric channel, parallel-sided ($y = \pm 0.5$) for $x < 0$ and exponential ($y = \pm 0.5\mathrm{e}^x$) for $x > 0$, so there was a small slope discontinuity at $x = 0$. The dimensions given by Patterson show that the corresponding value of ϵ was 0.05, and he used Reynolds numbers in the range $19 < Re < 75$.)

If the flow in the channel is non-unique then we would expect there to be at least

three solution branches, one in which the flow separates on one wall and remains attached on the other, one in which the roles of the walls are reversed, and one in which the flow is separated on both walls, separation occurring at the same value of x on each (Borgas & Pedley 1990). In practice the last, 'symmetric' flow is likely to be unstable and unrealized. However, a series solution of the boundary layer equations (1.5) and (1.2) will inevitably lead to this symmetric solution for all values of ϵRe. This can be seen from the symmetry of the problem, when recast in terms of the new y-variable $y' = y - [1+F(x)]/2$, together with the symmetry of the leading term (1.6). Asymmetry can be achieved from the boundary layer equations only when ϵRe is taken to be $O(1)$ from the start, so that the leading-order equations admit eigensolutions.

In this paper we seek to introduce asymmetry by investigating the first correction to the series solution for non-vanishing ϵ^2. Formally, the $O(\epsilon^2)$ correction involves inclusion of all terms in (1.3) and (1.4) except for the v_{xx} term in (1.4). However, since we are interested in the properties of the series solution at large values of ϵRe, the dominant $O(\epsilon^2)$ correction is the inertial contribution to the cross-stream pressure gradient:

$$\epsilon^3 Re(uv_x + vv_y) = -p_y. \tag{1.9}$$

We continue to neglect the u_{xx} term in (1.3), and all the viscous terms in (1.4) (the equations are not the same as the 'parabolized Navier–Stokes equations' because of the continued neglect of v_{yy} in (1.4), though they are clearly parabolic in x). It should be recognized that this approach, while introducing asymmetry to the flow because of the asymmetry of the channel boundaries, will still lead to a unique solution.

A similar series solution approach to channel flow has previously been developed by a student of Van Dyke's, though his thesis (Lucas 1972) was not published. In fact, Lucas proposed a double series expansion for the full Navier–Stokes equations (1.2)–(1.4) in symmetric channels: in powers of ϵ for $Re = O(1)$ and then in powers of Re. However, the complicated recurrence relations for the coefficients in the series (involving further power series in y and in F and its derivatives) required so much computer storage that he was in practice unable to proceed beyond ϵ^{12}, and hence also Re^{12} (the five-dimensional array of coefficients at $O(\epsilon^{12})$ contained 227 018 terms). The problem was simplified somewhat for particular choices of the wall shape function $F(x)$, but truncating the series at ϵ^{12} proved not to provide adequate accuracy at values of ϵ large enough for separation to be predicted, even after the use of Padé approximants to extend the validity of the series. Lucas made more satisfactory progress in the limit $R \to \infty$, $\epsilon Re = O(1)$, when the equations are reduced to the boundary layer form (1.2) and (1.5). Our approach is in that case the same as his except that we have a more systematic way of generating some of the recurrence relations (see below) and the choice (1.7), (1.8) for $F(x)$ was not one of his. Moreover the extension to include the cross-stream pressure gradient (1.9) was not made by him.

In a related approach to the analysis of internal flow separation, Fraenkel (1962, 1963) proposed a generalization of lubrication theory in which, at every x, the channel walls could be regarded as approximately straight but non-parallel and the flow as one of the Jeffery–Hamel flows appropriate to their angle of divergence and to the Reynolds number. Separation could thus arise naturally, since Jeffery–Hamel flows can exhibit a separated character. Using a Jeffery–Hamel flow as the leading term in a series expansion, however, would be impractical because it is analytically too complicated.

An outline of the rest of this paper is as follows. In § 2 we develop the series solutions and use them to predict the x-locations ($x = x_s$) at which the wall shear becomes zero (taken to be equivalent to flow separation in these steady flows) for the geometry given by (1.7) and (1.8). Symmetry of the flow about $y = [1+F(x)]/2$ is not imposed, so its emergence from the problem without cross-stream pressure gradient is a check on the accuracy of the procedure. The development of asymmetry when the cross-stream pressure gradient is included is investigated. In § 3 we present direct finite difference solutions of various problems: (*a*) the boundary layer equations (1.2) and (1.5), confirming the values of x_s for the geometry (1.7) and (1.8), and failing to find an asymmetric solution for a wide but not exhaustive range of parameter values; and (*b*) the full Navier–Stokes equations for Reynolds numbers up to 500 and for a geometry given by (1.7) but with a different $g(x)$ at large x because it is necessary for the channel to become parallel-sided again as $x \to \infty$ in order that sensible downstream boundary conditions can be imposed. Comparison and discussion of the results are given in § 4.

2. Series solutions

(*a*) *Boundary layer equations: general theory*

If the velocity components are represented in terms of a stream function ψ, so that $u = \psi_y$, $v = -\psi_x$, the boundary-layer vorticity equation (the y-derivative of (1.5)) becomes

$$\psi_{yyyy} = \delta(\psi_y\psi_{yyx} - \psi_x\psi_{yyy}), \tag{2.1}$$

where $\delta = \epsilon Re$. Together with the boundary conditions,

$$\psi = \psi_y = 0 \quad \text{on} \quad y = 0; \qquad \psi = 1, \quad \psi_y = 0 \quad \text{on} \quad y = F(x), \tag{2.2}$$

equation (2.1) is to be solved as a power series in δ. We first transform the y-coordinate to $\eta = y/F(x)$, so that the upper boundary is $\eta = 1$ and (2.1) becomes

$$\psi_{\eta\eta\eta\eta} = \delta\{F(\psi_\eta\psi_{\eta\eta x} - \psi_x\psi_{\eta\eta\eta}) - 2F'\psi_\eta\psi_{\eta\eta}\}, \tag{2.3}$$

where $F' \equiv \mathrm{d}F/\mathrm{d}x$. A solution is attempted of the form

$$\psi = \sum_{n=0}^{\infty} \delta^n \psi_n(x,\eta), \tag{2.4}$$

where all the ψ_n satisfy homogeneous boundary conditions in η except $\psi_0(x,1) = 1$. The first three terms in the series are

$$\psi_0 = 3\eta^2 - 2\eta^3, \tag{2.5a}$$

$$\psi_1 = \frac{3F'}{35}(-\eta^2 + 3\eta^3 - 7\eta^5 + 7\eta^6 - 2\eta^7), \tag{2.5b}$$

$$\begin{aligned}\psi_2 = {} & \frac{18FF''}{35}\left(\frac{1}{9\cdot 77}\eta^2 - \frac{13}{60\cdot 77}\eta^3 - \frac{1}{60}\eta^5 + \frac{1}{20}\eta^6 - \frac{1}{70}\eta^7\right. \\ & \left. - \frac{1}{12}\eta^8 + \frac{1}{9}\eta^9 - \frac{1}{18}\eta^{10} + \frac{1}{99}\eta^{11}\right), \\ & - \frac{6F'^2}{35}\left(\frac{79}{120\cdot 77}\eta^2 - \frac{13}{15\cdot 77}\eta^3 - \frac{1}{5}\eta^5 + \frac{11}{20}\eta^6 - \frac{9}{35}\eta^7\right. \\ & \left. - \frac{5}{8}\eta^8 + \frac{11}{12}\eta^9 - \frac{7}{15}\eta^{10} + \frac{14}{165}\eta^{11}\right).\end{aligned} \tag{2.5c}$$

PHILOSOPHICAL TRANSACTIONS OF THE ROYAL SOCIETY A MATHEMATICAL, PHYSICAL & ENGINEERING SCIENCES

Subsequent terms involve more functions of x and a rapidly increasing number of powers of η; it is clearly impracticable to calculate them by hand. Enumerating the functions of x is possible, since for each n, the different functions involve all possible combinations of n functions multiplied together, with n derivatives (e.g. ψ_3 involves F^2F''', $FF'F''$ and F'^3; ψ_4 involves F^3F^{iv}, $F^2F'F'''$, $F^2F''^2$, FF'^2F'', F'^4; etc.). Thus the functions of x in ψ_n span all members of the set,

$$G_{nj}(x) = F^{a_0}F'^{a_1}F''^{a_2}\dots F^{(n)a_n}, \tag{2.6}$$

where the a_m are non-negative integers satisfying the diophantine equations,

$$\sum_{m=0}^{n} a_m = \sum_{m=1}^{n} m a_m = n. \tag{2.7}$$

If the number of such 'partitions' of n, satisfying (2.7), is $p(n)$, then the integer j in (2.6) runs from 1 to $p(n)$. For any n the partitions can be enumerated systematically in a variety of ways; we have used the elegant algorithm of Gupta (1980).

We seek a way of representing ψ_n as a finite double sum of known functions of x and functions of η, the coefficients of which satisfy an algorithm that can be programmed into the computer. Because of the difficulty of specifying in advance which of the functions $G_{nj}(x)$ will arise from each of the $G_{n-1,j}(x)$, it proves more convenient not to set

$$\psi_n(x,\eta) = \sum_{j=1}^{p(n)} G_{nj}(x) \sum_{k} f_{njk}(\eta)$$

but instead to write

$$\psi_n(x,\eta) = \sum_{k=2}^{4n+1} (1-\eta)^2 \eta^k g_{n,k}(x), \tag{2.8}$$

where the functions $g_{n,k}(x)$ can in principle be expressed as sums of the $G_{nj}(x)$. Note that (2.8) automatically satisfies the boundary conditions at $\eta = 0$, 1. Substitution of (2.4) and (2.8) into (2.3), and equating the coefficients of η^{J-3} gives the following recurrence relation for $g_{n+1,J}(x)$:

$$\begin{aligned}(J+1)J(J-1)(J-2)&[g_{n+1,J+1} - 2g_{n+1,J} + g_{n+1,J-1}] \\ &= \sum_{l=1}^{n-1}\sum_{k=2}^{4l+1} g_{lk} \sum_{i=0}^{4} (p_i^{k,J-k-i} F g'_{n-l,J-k-i} + q_i^{k,J-k-i} F' g_{n-l,J-k-i}) \\ &\quad + \sum_{i=0}^{3} (r_i^{J-2-i} F g'_{n,J-2-i} + s_i^{J-2-i} F' g_{n,J-2-i}),\end{aligned} \tag{2.9}$$

where $p_i^{k,k'}$, $q_i^{k,k'}$, r_i^k, s_i^k are constants defined as follows:

$$\begin{aligned}\sum_{i=0}^{4} q_i^{k,k'} \eta^i &= -2(1-\eta)[k-(k+2)\eta][k'(k'-1) - 2(k'+1)k'\eta + (k'+2)(k'+1)\eta^2] \\ &= Q(k,k',\eta), \quad \text{say;} \\ \sum_{i=0}^{4} p_i^{k,k'} \eta^i &= -\tfrac{1}{2}Q(k,k',\eta) - k(1-\eta)[k(k-2) - 2(k^2-1)\eta + (k+2)(k+1)\eta^2];\end{aligned}$$

$$\sum_{i=0}^{3} r_i^k \eta^i = 6(1-\eta)[k(k-1) - 2(k^2+k-1)\eta + (k+3)k\eta^2];$$

$$\sum_{i=0}^{3} s_i^k \eta^i = -12(1-\eta)[k^2 - (2k+1)(k+2)\eta + (k+3)(k+2)\eta^2].$$

In (2.9) the index J is taken in the range $J = 3, 4 \ldots (4n+6)$, but on the left-hand side the functions $g_{n+1,J}$ are identically zero if $J > 4n+5$, while on the right-hand side the functions $g_{n-l,J-k-i}$ are non-zero only if $2 \leqslant J-k-i \leqslant 4(n-l)+1$ (from (2.8)). For each n, putting $J = 4n+6$ gives $g_{n+1,4n+5}$ in terms of the $g_{l,k}$ with $1 \leqslant l \leqslant n$, then $J = 4n+5$ gives $g_{n+1,4n+4}$, etc., down to $J = 3$ which gives $g_{n+1,2}$. The functions $g_{nk}(x)$, $n = 1, 2$, $k = 2, 3 \ldots 4n+1$ have been calculated explicitly as a check on the computations (a list can be obtained from the authors on request).

In order to learn about flow separation we need to compute the dimensionless shear rate (vorticity) as a function of position on the two walls, $\tau_0(x)$ on $y = 0$ and $\tau_1(x)$ on $y = F(x)$. Now

$$\tau_0(x) = \left.\frac{\partial u}{\partial y}\right|_{y=0} = \psi_{yy}|_{y=0} = \frac{1}{F^2(x)} \sum_{n=0}^{\infty} \delta^n \psi_{n\eta\eta}\Big|_{\eta=0} \tag{2.10}$$

and, to leading order in ϵ^2, $\tau_1(x)$ is equal to the negative of the same quantity evaluated at $\eta = 1$. From (2.8) we further have (for $n \geqslant 1$)

$$\psi_{n\eta\eta}|_{\eta=0} = 2g_{n2}(x) \tag{2.11 a}$$

while

$$-\psi_{n\eta\eta}|_{\eta=1} = -\sum_{k=2}^{4n+1} 2g_{nk}(x). \tag{2.11 b}$$

As pointed out above, these two quantities must be equal for all x, but as a check on the accuracy of the computations we did not assume equality *a priori*.

Automatic implementation of the algorithm (2.9) requires knowledge of the functions g_{lk} each of which contains many terms of the form (2.6) involving $F(x)$ and its derivatives. We write

$$g_{nk}(x) = \sum_{j=1}^{p(n)} a(n,k,j) G_{nj}(x), \tag{2.12}$$

where each of the $G_{nj}(x)$ corresponds to one partition of n. We then note that the right-hand side of the recurrence relation (2.9) yields sums of terms of the form $Fg_{lk}g'_{mk'}$, $F'g_{lk}g_{mk'}$, Fg'_{nk}, $F'g_{nk}$, where $m = n-l$, $k' = J-k-1$. In order to express the $g_{n+1,k}$ in a form similar to (2.12) it is necessary to regroup and re-order all these terms, noting that

$$G'_{nj} = \sum_{i=0}^{n} a_i (F^{(i+1)}/F^{(i)}) G_{nj},$$

so that they correspond systematically to the partitions of $n+1$, previously enumerated and listed in a data-file. When the terms have been regrouped, the coefficients can be derived by simple addition, and the $a(n+1,k,j)$ computed using (2.9). It should be noted that the $a(n,k,j)$ are *universal* coefficients, applicable for any wall shape.

The accurate implementation of this procedure, for a general function $F(x)$, requires extremely large computer storage and time, and round-off errors rapidly become severe, especially for the calculation of τ_1. We have calculated the coefficients $a(n,k,j)$ for values of n up to 11, which indirectly requires the generation of $4\sum_{m=1}^{11} mp(m) = 6888$ coefficients. The number of required coefficients is lower than in Lucas's (1972) method, but accuracy is not markedly improved. The wall shears τ_0 and τ_1 were computed as functions of x for two different wall shapes, that given by (1.7) and (1.8), and

$$F(x) = 1 - \beta \mathrm{e}^{-x^2}. \tag{2.13}$$

Results for the exponential channel are given in the next section. Results for the channel given by (2.13) are shown in figure 2. The value of β was taken to be 0.4, and values of δ from 1.0 to 3.0 were taken. Figure 2*a* shows graphs of $\tau_0(x)$ and $\tau_1(x)$ for $\delta = 1.0$. The curves for $N = 7$, 8, 9 were indistinguishable. It can be seen, however, that even at such a low value of δ, there is a small discrepancy between τ_0 and τ_1, attributable to round-off error in the calculation of the latter. At $\delta = 1.5$ (figure 2*b*) the discrepancy has grown much bigger, and at $\delta = 2.0$ (not shown) the results for τ_1 were completely unacceptable. By $\delta = 2.5$, the results for τ_0 also showed unphysical variations (figure 2*c*) and are therefore unacceptable. Differences between the results truncated at different values of N were becoming apparent at this value of δ. Improvement of convergence by Padé approximants is described below, for the exponential channel only.

(*b*) *Boundary layer equations: exponential channel*

In order to make numerical progress without unmanageable requirements in computer storage or time, we now restrict attention to the channel shape given by (1.7) and (1.8). In fact, if we write $f(x) = \beta \mathrm{e}^x$ we see that $F \equiv 1 + f$ but all the derivatives of F are identically equal to f. In this case all the functions of x appearing in $\psi_n(x,\eta)$ (cf. the functions $G_{nj}(x)$ in (2.6)) are of the form $f^j(1+f)^{n-j}$ with $1 \leqslant j \leqslant n$. It therefore makes sense to write (for $n \geqslant 1$)

$$\psi_n(x,\eta) = \sum_{l=1}^{n} f^l(x)\phi_{n,l}(\eta), \tag{2.14}$$

so that substitution into the equations gives the following equation for $\phi_{n+1,l}$ in terms of the $\phi_{j,k}$ with $1 \leqslant j \leqslant n$:

$$\begin{aligned}\phi^{\mathrm{iv}}_{n+1,l} = {} & l\phi_0'\phi''_{n,l} + (l-3)\phi_0'\phi''_{n,l-1} - l\phi_0'''\phi_{n,l} - (l-1)\phi_0'''\phi_{n,l-1} \\ & -2\phi_0''\phi'_{n,l-1} + \sum_{j=1}^{n-1}\sum_{k=k_1}^{k_2} k(\phi''_{j,k}\phi'_{n-j,l-k} - \phi_{j,k}\phi'''_{n-j,l-k}) \\ & + \sum_{j=1}^{n-1}\sum_{k=\tilde{k}_1}^{\tilde{k}_2}[(k-2)\phi''_{j,k}\phi'_{n-j,l-1-k} - k\phi_{j,k}\phi'''_{n-j,l-1-k}] \end{aligned} \tag{2.15a}$$

for $3 \leqslant l \leqslant n$, where $\phi_0(\eta) \equiv \psi_0(\eta)$ in (2.5*a*) and

$$\begin{aligned} k_1 &= \max[1, l+j-n], & k_2 &= \min[j, l-1], \\ \tilde{k}_1 &= \max[1, l-1+j-n], & \tilde{k}_2 &= \min[j, l-2]. \end{aligned}$$

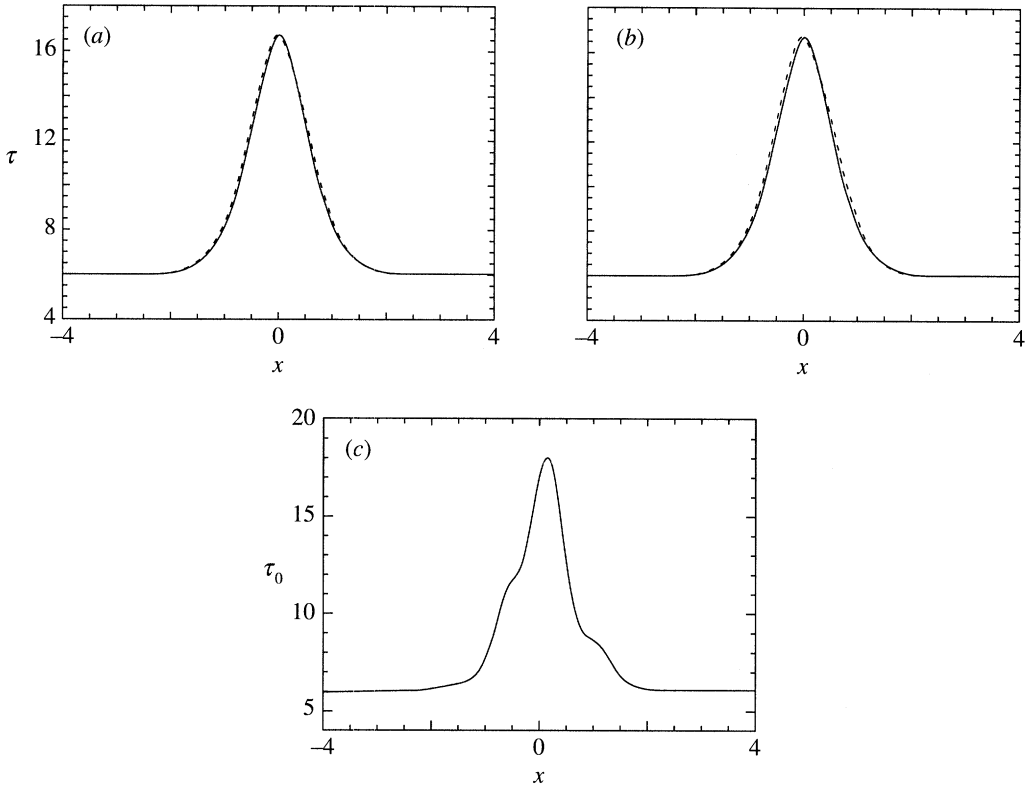

Figure 2. Dimensionless wall shear magnitude as a function of x, computed using the direct sum of 7, 8 or 9 terms of the series expansion for a channel with $F(x) = 1 - \beta e^{-x^2}$. Solid curves, shear on plane wall (τ_0); broken curves, shear on non-planar wall (τ_1). (*a*) $\delta = 1$, (*b*) $\delta = 1.5$, (*c*) $\delta = 2.5$.

At the ends of the range of l we also have

$$\phi^{\mathrm{iv}}_{n+1,1} = \phi'_0\phi''_{n,1} - \phi'''_0\phi_{n,1}, \tag{2.15 b}$$

$$\phi^{\mathrm{iv}}_{n+1,2} = 2\phi'_0\phi''_{n,2} - \phi'_0\phi''_{n,1} - 2\phi'''_0\phi_{n,2} - \phi'''_0\phi_{n,1} - 2\phi''_0\phi'_{n,1} + \sum_{j=1}^{n-1}(\phi''_{j,1}\phi'_{n-j,1} - \phi_{j,1}\phi'''_{n-j,1}), \tag{2.15 c}$$

$$\phi^{\mathrm{iv}}_{n+1,n+1} = (n-2)\phi'_0\phi''_{n,n} - n\phi'''_0\phi_{n,n} - 2\phi''_0\phi_{n,n} + \sum_{j=1}^{n-1}[(j-2)\phi''_{j,j}\phi'_{n-j,n-j} - j\phi_{j,j}\phi'''_{n-j,n-j}]. \tag{2.15 d}$$

Note that $\phi_{1,1}(\eta) \equiv \psi_1(\eta)$ in (2.5*b*). The boundary conditions on the $\phi_{n,l}$ are that $\phi_{n,l}$ and $\phi'_{n,l}$ are zero at $\eta = 0$, 1. In terms of these functions, the wall shear rates are determined by $\phi''_{n,l}(\eta)$ evaluated at $\eta = 0$ and 1.

One approach to the numerical evaluation of the required quantities would be to represent the $\phi_{n,l}$ as polynomials in η, and automate the evaluation of the coefficients, as done above and by Lucas (1972) for the more general wall shapes. $\phi_{2,1}(\eta)$ and $\phi_{2,2}(\eta)$ have been calculated explicitly, but it is easier to do the integrations

Table 1. *Values of $\phi''_{n,l}(0)$ at selected values of n, l*

(For each $n > 3$, the value of l was chosen for which the magnitude of $\phi''_{n,l}(0)$ was greatest. Results are given for three different values of M so that accuracy can be assessed.)

		$\phi''_{n,l}(0)$		
n	l	$M = 30$	$M = 40$	$M = 50$
1	1	0.17143 E 00	0.17143 E 00	0.17143 E 00
2	1	0.14702 E−02	0.14765 E−02	0.14842 E−02
2	2	−0.14525 E−02	−0.14507 E−02	−0.14471 E−02
3	1	−0.17984 E−04	−0.18000 E−04	−0.18023 E−04
3	2	0.87942 E−04	0.87649 E−04	0.87300 E−04
3	3	0.10944 E−04	0.10909 E−04	0.10928 E−04
4	2	−0.29565 E−05	−0.29415 E−05	−0.29232 E−05
5	2	0.85881 E−07	0.85233 E−07	0.84451 E−07
6	3	0.40098 E−08	0.39537 E−08	0.38842 E−08
10	6	0.27865 E−13	0.27184 E−13	0.26356 E−13
15	10	−0.33858 E−17	−0.33062 E−17	−0.31854 E−17
19	13	−0.14585 E−19	−0.14480 E−19	−0.13950 E−19

in (2.15) directly by a finite difference method, dividing the region $0 \leqslant \eta \leqslant 1$ into M equal intervals. At each n it is necessary to store the values of $\phi_{n,l}$ and its first three derivatives at all $M + 1$ grid points, which makes $2n(n + 1)$ functions needed to evaluate the right-hand sides of (2.15*a–d*). We would like to take the series to large values of n (though in this work we have gone only as far as $n = 19$), and the integration, although simple, becomes very time-consuming. It is therefore desirable to make M as small as possible. On the other hand great accuracy is needed for series manipulation techniques, which requires not only quadruple precision but also as large a value of M as possible. In the event we used h^2-accurate central difference formulae, improved by Richardson extrapolation to give $O(h^4)$ accuracy (Keller 1968), and took $M = 50$. To calculate the derivatives at the end points, values of the function at external points were taken to be the same as at the corresponding internal points (because of the boundary conditions). Accuracy was assessed by repeating the procedure for other values of M (30 and 40) and comparing the results (see the discussion of table 1 below).

The wall shear rate at $\eta = 0$ is given by (2.11) to be

$$\tau_0 \approx \frac{1}{(1+f)^2}\left\{6 + \sum_{n=1}^{N} \delta^n \sum_{l=1}^{n} f^l(x)\phi''_{n,l}(0)\right\}, \tag{2.16}$$

for some value of N to be chosen, and there is a similar expression for τ_1. The results of the above numerical procedure can then be summarized in tables of values of $\phi''_{n,l}(0)$ and $\phi''_{n,l}(1)$. These derivatives are calculated from difference tables of the values of the functions stored at the grid points. Numerical errors in these tables are minimized by means of a filtration procedure using a least squares approximation and cubic splines (Hildebrand 1991). Then Markov's expansion (Lowan *et al.* 1942)

is used for the second derivative in terms of advancing differences $\Delta^n\phi$; where ϕ is a generic function:

$$h^2D^2\phi = \sum_{j=2}^{\infty}(-1)^{j-2}N_{2,j}\Delta^k\phi,$$

where $N_{2,2} = 1$, $N_{0,j} = 0$ $(j > 0)$, $N_{1,j} = 1/j$ and

$$(j+1)N_{2,j+1} = jN_{2,j} + 2N_{1,j}.$$

Results from the computations are given in table 1 for selected values of n and for the values of l which, for each selected n, correspond to the largest magnitude of $\phi''_{n,l}(0)$. The differences in the values for different numbers of grid-points, M, are nowhere more than 6%, even for the larger values of n for which inaccuracy might be expected to be greater. The values of $\phi''_{n,l}(1)$ were also computed and were, as expected, found to be the negative of $\phi''_{n,l}(0)$, accurate to eight significant figures for $n = 4$, falling to four significant figures for $n = 19$. It can be seen that the magnitude of $\phi''_{n,l}(0)$ falls sharply as n increases, suggesting that convergence of the series (2.16) may be quite good for values of δ and f that are not extremely small.

The object of the study is to find the values of x at which separation occurs, in particular at relatively large values of the Reynolds number Re. The position and geometry are represented by $f(x) = \beta e^x$ (note, too, that β is essentially arbitrary, since if $\beta = e^{-x_0}$ we see that a change in β is equivalent to a change in origin x_0), which also incorporates a definition of the longitudinal length-scale ϵ^{-1}, while Re is specified by $\delta = \epsilon Re$. It would therefore seem desirable to reorder the sums in (2.16), to

$$\sum_{l=1}^{N} f^l \sum_{n=l}^{N} \delta^n \phi''_{n,l}(0),$$

so that δ can be specified and f varied simply. However, this means that the sum for every value of Re involves values of the functions up to $n = N$, and the larger values of n are inevitably less accurately determined. We therefore retain the ordering in (2.16), choosing particular values of f before manipulating the series in powers of δ.

For a given value of f, then, we compute

$$A_I(f,n) = \sum_{l=1}^{n} f^l \phi''_{n,l}(I), \qquad I = 0, 1$$

and consider

$$\sigma_I^{(N)} = \sum_{n=1}^{N} \delta^n A_I(f,n), \tag{2.17}$$

where $(1+f)^2\tau_I = 6\,\mathrm{sgn}\, I + \sigma_I$. Values of $A_0(f,n)$ are given for a few values of f in table 2; the $A_0(f,n)$ clearly decrease in magnitude as n increases if f is small enough. However, we see from table 2 that for the values of f chosen here the decrease ceases after about $n = 8$, when a regular alternation in sign begins. For higher n the magnitude of $A_0(f,n)$ starts to increase again; indeed for f as high as 17.88 ($\beta = 0.4$, $x = 3.8$) the values of A_0 start to blow up rapidly by $n = 19$. The values of $A_1(f,n)$ are again found to be the negative of $A_0(f,n)$, the first error appearing in the fourth, fifth or sixth significant figure for different values of n. It is clear that the direct sums will fail to converge when δ exceeds a particular value that depends

Table 2. *Values of $A_0(f,n)$ for $f=\beta e^x$ where $\beta=0.4$ and x takes different values*

	$A_0(f,n)$	
n	$x=2.91$	$x=3.51$
1	−0.12588 E+01	−0.22936 E+01
2	−0.67125 E−01	−0.23919 E 00
3	0.89007 E−02	0.41558 E−01
4	0.19039 E−02	0.21038 E−01
5	−0.86242 E−04	−0.25339 E−03
6	−0.23094 E−04	−0.82254 E−03
7	−0.50381 E−05	−0.35443 E−03
8	0.23287 E−05	0.19653 E−03
9	−0.98391 E−06	−0.14440 E−03
10	0.69665 E−06	0.19356 E−03
11	−0.54757 E−06	−0.26889 E−03
12	0.48183 E−06	0.42006 E−03
13	−0.47517 E−06	−0.73611 E−03
14	0.51792 E−06	0.14243 E−02
15	−0.61823 E−06	−0.30168 E−02
16	0.80216 E−06	0.69437 E−02
17	−0.11241 E−05	−0.17258 E−01
18	0.16922 E−05	0.46063 E−01
19	−0.27232 E−05	−0.13142 E 00

on f (or x): at $x=3.51$, for example, the 19th term of the series (2.17) is bigger than all the other terms except the first two for $\delta=1.0$, while even at $x=2.60$, the 19th term is bigger than the leading term for $\delta \gtrsim 2.6$. Calculation shows that when convergence fails the magnitude of σ_I is still less than 6, so flow separation has not occurred (see figure 3 below).

In order to increase the values of δ for which converged results can be obtained, we seek to recast the series (2.17) in a different form. The nature of the singularity (in the complex δ-plane) which limits the convergence of a series such as (2.17) can often be estimated by extrapolating the Domb–Sykes plot, of $|A_0(f,n)/A_0(f,n-1)|$ against $1/n$ (Van Dyke 1975), to $1/n=0$. An Euler transformation can then be used to remove the singularity to infinity. In this case, however, the Domb–Sykes plot did not become approximately a straight line and accurate extrapolation was impossible (Lucas (1972) had the same difficulty). Instead we have used the technique of Padé approximants which approximately represent an analytic continuation of the function (of δ) given by the series, outside the radius of convergence of the series. The approximation is invariant under an Euler transformation and yields a result at least as good as can be achieved by the best Euler transformation (Baker 1975; Graves-Morris 1973; Van Dyke 1984). The Padé sums P_m^{m+j} $(j=0,\,1)$ provide estimates of the sum of the series that improve as m is increased (the maximum value of m is

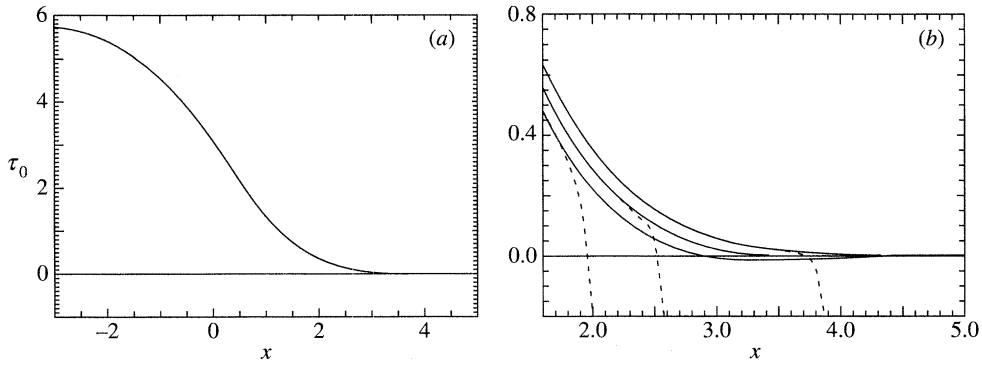

Figure 3. Dimensionless wall shear magnitude as a function of x for the exponentially diverging channel. (a) Direct and Padé sums for $\delta = 1$. (b) A detail of (a), with similar curves for $\delta = 3$ and $\delta = 5$. Solid curves, Padé sum; broken curves, direct sum.

limited by the value of N in (2.17)). Experience has shown that both convergence and accuracy are much better than for the direct sums, and hence we can obtain accurate estimates of wall shear at a given value of f (i.e. x) for considerably larger values of δ.

The results can be presented either as computed, i.e. to see where the Padé sums break down as δ is increased for fixed f and whether flow separation occurs before that, or the other way round, i.e. vary f for a given δ. We choose the latter approach as it corresponds more clearly with experimental feasibility. Examples of the resulting estimates for τ_0 (equation (2.16)) are given in table 3 for three values of δ (= 1.0, 3.0, 5.0) and for several values of f, including those for which the direct sum failed to converge. The results are also plotted in figure 3. In table 3, the values of τ_0 are given to five decimal places except where the Padé sums do not converge to so many decimal places; in those cases the converged results are given. The corresponding values computed for $-\tau_1$ are identical to those presented here for τ_0. The results are most encouraging: converged results can be achieved all the way to values of x at which the wall shear reverses, and (with lower accuracy) for some distance beyond. Accuracy is generally lower for higher values of δ, but it still reasonable to beyond the point of shear reversal, for $\delta = 5.0$. The plotted graph of $\tau_0(x)$ in figure 3a, for $\delta = 1$, differs everywhere by less than 0.02 from the lubrication theory result ($\delta = 0$). In the neighbourhood of the separation point, however, where the magnitude of τ_0 is less than 0.02, this makes a large difference. Figure 3b, with an expanded abscissa, shows the differences in $\tau_0(x)$ for various values of δ (= 1, 3, 5): the curves are close to each other, but the position of the separation point varies considerably. The separation point x_s can be estimated from such graphs and is listed for various values of δ in table 4, for comparison with the other numerical results described in § 3.

One interesting feature of the results in table 3 or figure 3 is that, after flow separation, the magnitude of the reversed wall shear reaches a (small) maximum and then starts to fall again, very slightly, with distance downstream. As we shall see, this is confirmed by direct computation (see figure 7 below).

(*c*) *Inclusion of cross-stream pressure gradient*

Including the leading cross-stream pressure gradient term (1.9) changes the governing equation (2.1) to

$$\psi_{yyyy} = \delta(\psi_y\psi_{yyx} - \psi_x\psi_{yyy}) + \epsilon^2\delta(\psi_y\psi_{xxx} - \psi_x\psi_{yxx}), \tag{2.18}$$

Table 3. *Padé sums (to $N = 19$) for τ_0, at various values of δ and x*

($f = 0.4e^x$. The direct sum (to $N = 19$) was meaningless at all these values of x except for $\delta = 1$ where it agreed to four decimal places up to $x = 3.35$, after which its convergence deteriorated rapidly. Results given to five decimal places or to the number for which the Padé sums converge, whichever is the less.)

x	$\delta = 1$	$\delta = 3$	$\delta = 5$
2.80			0.0050
2.82			0.0031
2.85	0.07605	0.03528	0.0005
2.86			−0.0003
2.90	0.06870	0.02945	−0.0033
3.00	0.05581		
3.05	0.05018	0.01542	−0.0111
3.10	0.04503	0.01176	−0.013
3.30	0.02865	0.00118	−0.016
3.33		0.00006	−0.016
3.34		−0.00029	−0.016
3.35	0.02544	−0.00062	−0.016
3.40	0.02253	−0.0021	−0.016
3.55	0.01536	−0.0052	−0.01
3.70	0.01011	−0.0065	−0.01
3.85	0.00631	−0.007	−0.01
4.00	0.00361	−0.006	
4.10	0.00230	−0.006	
4.20	0.00128		
4.25	0.00088		
4.30	0.00052		
4.40	−0.00003		
4.45	−0.00025		
4.50	−0.00042		
4.60	−0.00068		
4.80	−0.00089		
5.00	−0.00086		

with an error of $O(\epsilon^2)$, smaller than $\epsilon^2\delta$ in the limit of large δ. In terms of the transformed variable η, and for the exponential channel ($F = 1 + f$, $f' \equiv f$), this is

$$\begin{aligned}\psi_{\eta\eta\eta\eta} = \delta\{&F(\psi_\eta\psi_{\eta\eta x} - \psi_x\psi_{\eta\eta\eta}) - 2f\psi_\eta\psi_{\eta\eta}\} + \epsilon^2\delta\{F^3(\psi_\eta\psi_{xxx} - \psi_x\psi_{\eta xx})\\ &+2fF^2(\eta\psi_x\psi_{\eta\eta x} + \psi_x\psi_{\eta x} - \eta\psi_\eta\psi_{\eta xx})\\ &+fF[\eta^2 f\psi_\eta\psi_{\eta\eta x} - \eta(3-f)\psi_\eta\psi_{\eta x} - \eta^2 f\psi_x\psi_{\eta\eta\eta} + \eta(1-3f)\psi_x\psi_{\eta\eta}\\ &+(1-f)\psi_x\psi_\eta] + \eta f\psi_\eta[2f\eta\psi_{\eta\eta} - (1-3f)\psi_\eta]\}. \qquad (2.19)\end{aligned}$$

The solution can again be expanded in powers of δ, and we write

$$\psi = \psi_0(\eta) + \sum_{n=1}^{\infty}\delta^n[\psi_n(x,\eta) + \epsilon^2\tilde{\psi}_n(x,\eta)] + o(\epsilon^2), \qquad (2.20)$$

Table 4. *Value of βe^x at separation for the exponential channel*

('τ_0' refers to the lower, plane, wall and 'τ_1', to the upper, curved, wall. The four columns represent the results of the series method without and with cross-stream pressure gradient (§ 2 *b* and 2 *c* respectively), direct numerical integration of the boundary layer equations (§ 3 *a*), and numerical solution of the Navier–Stokes equations (§ 3 *b*). Under 'num.N.S.', S refers to the 'symmetric' solution, A1 to the solution with first separation on the upper wall and A2 to that with first separation on the plane lower wall. In all cases $f = 1 + \beta e^x$ with $\beta = 0.4$; for the Navier–Stokes calculation, $\epsilon = 0.01$, $Re = \delta/\epsilon$.)

					num.N.S.		
δ		series (Padé)	series (cross-stream)	num.b.l.	S	A1	A2
1.0	τ_0		35.2				
		32.6		32.19	none		
	τ_1		34.9				
3.0	τ_0		11.6		11.08	9.81	—
		11.2		11.09			
	τ_1		11.5		11.08	—	9.77
5.0	τ_0		7.02			6.11	—
		6.9		6.87			
	τ_1		6.76			—	6.12

where ψ_n is given by (2.14) and the results of § 2 *b*, and

$$\tilde{\psi}_n = \sum_{l=1}^{n+2} f^l(x)\tilde{\phi}_{n,l}(\eta) \tag{2.21}$$

(cf. equation (2.14)). The leading terms are

$$\tilde{\phi}_{1,1} = -\left(\frac{\eta^2}{35} - \frac{17\eta^3}{420} + \frac{3\eta^7}{70} - \frac{3\eta^8}{70} + \frac{\eta^9}{84}\right),$$

$$\tilde{\phi}_{1,2} = \frac{\eta^2}{14} - \frac{47\eta^3}{420} + \frac{3\eta^7}{14} - \frac{9\eta^8}{35} + \frac{\eta^9}{12},$$

(with $\tilde{\phi}_{1,3} \equiv 0$) and both these functions have the property that $\tilde{\phi}''_{1,i}(0) \neq -\tilde{\phi}''_{1,i}(1)$. In other words, the contribution to the wall shear rate is different on the two walls and asymmetry is inevitable.

The terms in (2.20) and the corresponding contributions to the wall shear can be computed systematically as for the $\phi_{n,l}$ in § 2 *b*. However, the number of terms on the right-hand side of (2.19) and in the series (2.20) makes the process much more cumbersome so further equations are omitted, though numerical integration of the ordinary differential equations for $\tilde{\phi}_{n,l}(\eta)$ has been carried out up to $n = 20$. We go straight to the resulting predictions of the wall shear. By analogy with (2.17), we define

$$B_I(f,n) = \sum_{l=1}^{3n-1} f^l \tilde{\phi}''_{n,l}(I), \qquad I = 0, 1$$

and compute the contributions

$$\tilde{\sigma}_I(N) = \sum_{n=1}^{N} \delta^n B_I(f, n)$$

for various values of δ and f; the wall shear on the two walls is given by

$$(1+f)^2 \tau_I = 6 \operatorname{sgn} I + \sigma_I + \epsilon^2 \tilde{\sigma}_I.$$

The direct sum was again not useful, and Padé approximants were used to improve the convergence of the series. The results have been interpreted as the values of x (and hence βe^x) at which separation occurs on the two walls, and are given in table 4 for $\epsilon = 0.01$, $\delta = 1, 3, 5$. It can be seen that the presence of the cross stream pressure gradient causes separation of the 'symmetric' flow to occur slightly earlier on the curved wall than on the plane wall, as one might expect. At $\delta = 1$ and 3, separation is predicted to be delayed by the presence of the cross-stream pressure gradient; however, since there has been no independent check on this prediction it should be treated with caution.

3. Finite difference solutions

(a) *Boundary layer equations*

The boundary layer problem was solved numerically in streamfunction-vorticity form, i.e. as

$$\omega = \frac{1}{(1+z)^2} \psi_{\eta\eta}, \qquad \delta z(1+z)(\psi_\eta \omega_z - \psi_z \omega_\eta) = \omega_{\eta\eta}, \tag{3.1}$$

where the (x, y) coordinate system has been transformed into a (z, η) one, where $z = \beta e^x$, and $\eta = y/(1+z)$, in accordance with (1.7) and (1.8); ω is the negative of the (boundary layer) vorticity. These equations were marched downstream from Poiseuille flow at $z = 0$ using a standard finite-difference method; in stepping from z_{j-1} to z_j, a Crank–Nicholson scheme was used for the vorticity transport equation with the vorticity definition enforced at z_j. Standard three-point difference formulae were used for the second derivatives, and the vorticity definition and the no-slip condition were used to obtain finite-difference formulae for the wall vorticity.

There was no difficulty in integrating (3.1) past the separation point, although, not surprisingly, the numerical procedure did break down eventually. The solutions obtained were always symmetric, with separation occurring at the same position on both walls. Symmetry was not explicitly enforced; indeed, an attempt was made to generate non-symmetric solutions by perturbing the starting values at $z = 0$. However, this initial non-symmetry was damped out well before separation occurred. Notwithstanding the analysis of Borgas & Pedley (1990), therefore, it must be regarded as extremely difficult to generate non-symmetric separation from the boundary layer equations in the absence of a cross-stream pressure gradient.

Computed values of the separation point, for various values of δ, can be found in table 4.

(b) *Navier–Stokes equations*

Again, the streamfunction-vorticity form of the Navier–Stokes equations was used. Since the problem is now elliptic rather than parabolic, suitable downstream bound-

ary conditions must be adopted. There are no obvious conditions to apply to the separated flow we would expect with a channel given by (1.7) and (1.8), and, therefore, we have modified the channel to

$$F(x) = 1 + \tfrac{1}{2}z(1 - \tanh(k(x - x_1))) + z_0\tfrac{1}{2}(1 + \tanh(k(x - x_1))). \qquad (3.2)$$

Initially this channel has an exponential expansion as before, but far downstream it takes the form of a uniform channel of width $1 + z_0$, so that we can assume in the numerical procedure that parallel flow exists at the downstream boundary. A $(\bar{x}, \eta)$ coordinate system was used, with $\eta = y/F$ and $\bar{x} = \epsilon^{-1}x$, so that $\bar{x}$ is the physical coordinate scaled on the upstream channel width.

A finite-difference scheme with central differences for the cross-stream convective term, and first order upwinding for the streamwise term, was used for the transformed equations. Upwinding on the streamwise convective terms was required to stabilize the iteration scheme; the grid step in $\bar{x}$ was necessarily large because of the length of the channel, and with central differences in $\bar{x}$ the iteration matrix was far from diagonally dominant and the numerical method was completely unstable. Upwinding greatly enhanced the diagonal dominance of the matrix. The difference equations were solved using a line implicit relaxation method, i.e. for each grid line across the channel (each $\bar{x}_j$) the difference equations for either the Poisson equation for the streamfunction or the vorticity transport equation were arranged to form a tridiagonal system connecting the variables lying on that grid line. These tridiagonal systems are easily solved to update the variables on each grid line. Complete sweeps through the grid were performed to update the streamfunction and vorticity in turn – this gives a faster convergence rate than updating both the streamfunction and vorticity on each line in the same sweep. At the downstream boundary the second derivatives with respect to $\bar{x}$ were set to zero. The process was repeated until $\Delta\psi$, the maximum absolute change in the streamfunction at any point on the grid, fell below a specified tolerance.

Calculations were performed for channels with $\beta = 1$, $\epsilon = 0.01$, $\bar{x}_{\min} = -500$, $\bar{x}_{\max} = 2000$, $k = \epsilon^{-1}$, and $z_0 = 20$, $x_1 = 3$ or $z_0 = 40$, $x_1 = 3.69$. With these values, the channel expansion is essentially monotonic, with only a slight overshoot where the channel changes shape. (The apparent abrupt change in shape shown in figures 4 and 6 below is deceptive; the change in shape is in fact smooth, and appears sharp only because of the scaling used for the figures.) With channels of the width used here, the downstream development of Poiseuille flow is slow (for the $(\bar{x}, y)$ coordinate system the dominant eigenvalue is $O(Re^{-1}(1+z_0)^{-1})$; see Wilson (1969)) and it was therefore necessary to place the downstream boundary relatively far downstream: $\bar{x}_{\max} = 2000$ was found to be sufficient for the channels considered here.

Three different Reynolds numbers were used, $Re = 100$, 300, and 500, giving $\delta = 1$, 3, and 5, respectively. With $Re = 100$ and $z_0 = 20$, the channel expansion ended before the flow could separate. The flow with $Re = 300$ was much more interesting, and three different branches of the solution were found. The initial approximation, scaled Poiseuille flow, was symmetric in η, and with 33 points across the channel ($\Delta\eta = \frac{1}{32}$) and 5001 along it ($\Delta\bar{x} = \frac{1}{2}$), the 'solution' at first remained quasi-symmetric as the iterations were performed, with $\Delta\psi$ decreasing monotonically. During this stage, separation bubbles were generated on the upper and lower walls, with the separation points at essentially the same position on both walls. However, as the iterations continued, $\Delta\psi$ reached a local minimum of approximately 5×10^{-5}, then increased for a time before finally decreasing again until the calculations were terminated when it fell

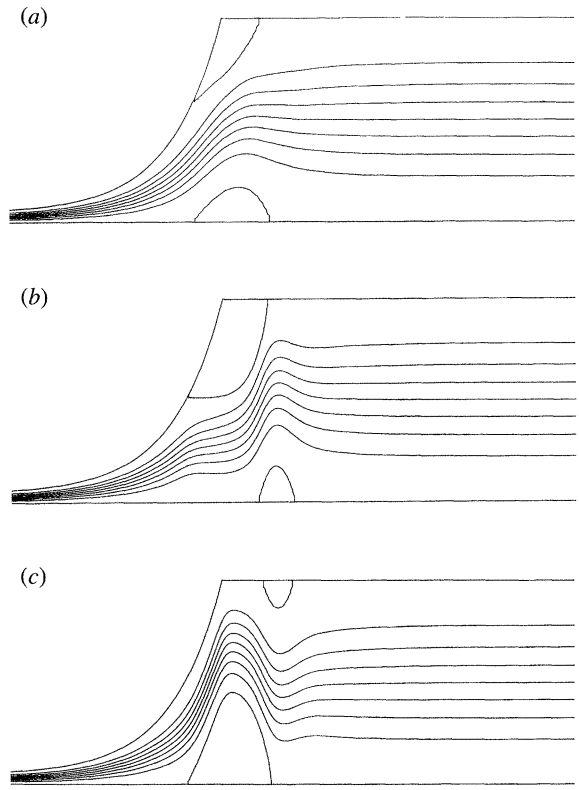

Figure 4. Streamline plots for $0 \leqslant \bar{x} \leqslant 1000$ from the Navier–Stokes calculation, with $\epsilon = 0.01$, $Re = 300$ ($\delta = 3$). (*a*) The not-quite-converged, approximately symmetric flow; (*b*) the converged flow with first separation on the upper wall; (*c*) the converged flow with first separation on the plane wall.

below 10^{-8}. At roughly the same stage in the iterative process that $\Delta\psi$ reached its (local) minimum, the maximum change in the vorticity, which is an order of magnitude less than $\Delta\psi$, also reached a local minimum, while as $\Delta\psi$ temporarily increased, the separation points on the upper and lower walls diverged, with that on the upper wall moving upstream and that on the lower wall moving downstream. Streamlines for the quasi-symmetric flow near the minimum in $\Delta\psi$ are shown in figure 4*a* and the shear rate, or vorticity, on the walls in figure 5*a*. (Somewhat arbitrarily these results were plotted for an iteration just before the separation points on the upper and lower walls diverged.) We note that, on the scale shown, the wall vorticity values of figure 5*a* are virtually the same as those obtained from the boundary layer solution with $\delta = 3$, as is the separation point (table 4).

When the calculation terminated, the flow pattern was markedly different from that shown in figure 5*a*, with separation predominantly on the upper wall (figure 5*b*), and occurring at a smaller value of x (table 4). Also, we generated a second fully converged solution with separation mainly on the lower wall (figure 5*c*), by using as a starting point the reflection about the centre-line of the channel of the solution with separation on the upper wall.

The solution structure described above is reminiscent of that found in a channel

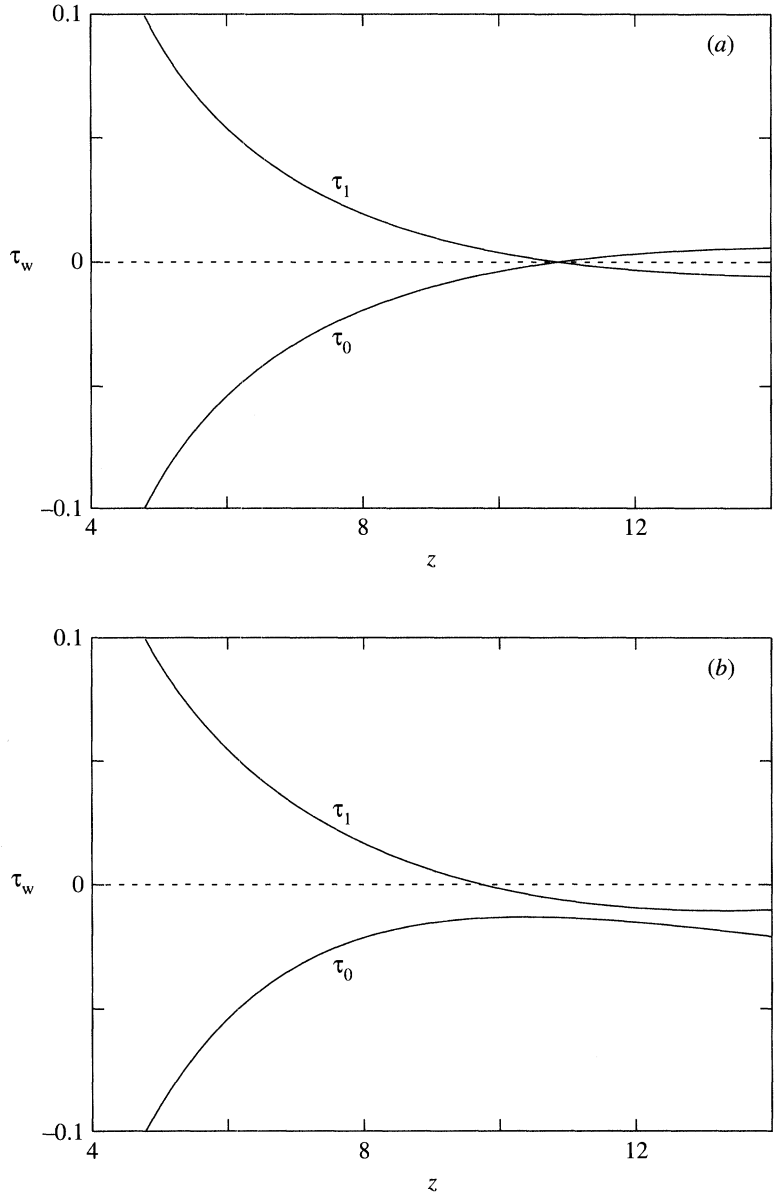

Figure 5. Wall shear (vorticity) plots corresponding to cases (*a*) and (*b*) of figure 4.

with a symmetric expansion, where there is a pitchfork bifurcation at a relatively low Reynolds number with a symmetric solution on the unstable central branch and two non-symmetric stable solutions which are mirror images of each other (Fearn *et al.* 1990; Borgas & Pedley 1990; Durst *et al.* 1993; etc.). Indeed, (unpublished) calculations by one of the authors (O.R.T.) in a channel with a symmetric 45° expansion have shown a similar pattern, in that initially the numerical procedure preferred the symmetric solution before switching to one of the non-symmetric branches. This, and the fact that the quasi-symmetric solution is by many standards well converged, leads us to the conclusion that, if the Reynolds number is large enough, there are

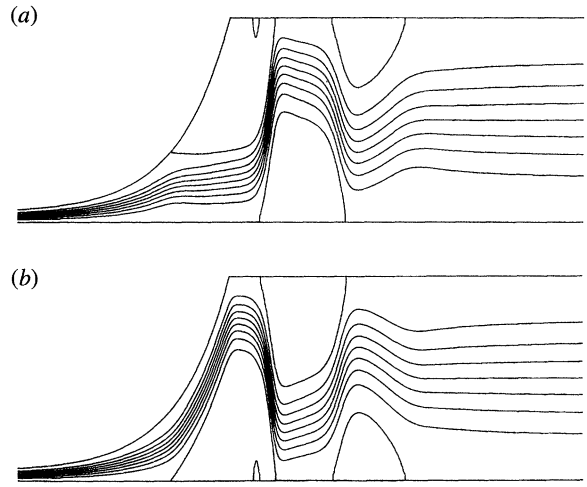

Figure 6. Streamline plots for $0 \leqslant \bar{x} \leqslant 1000$ and $\epsilon = 0.01$, $Re = 500$ ($\delta = 5$). (a) First separation on upper wall; (b) first separation on plane wall.

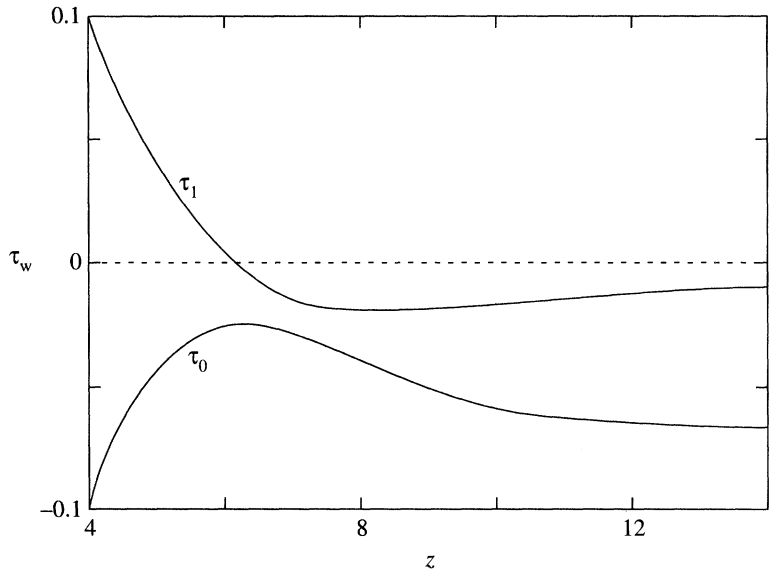

Figure 7. Wall shear (vorticity) plot corresponding to figure 6a.

in fact three distinct branches to the solution; the quasi-symmetric solution which is the analogue of the boundary layer solution but would not be obtained in practice, the preferred solution with the first separation on the upper wall, and the second stable solution with separation on the lower wall.

A similar pattern was found with $Re = 500$, though the quasi-symmetric solution did not converge sufficiently for results to be plotted. Streamlines for the two non-symmetric solutions are shown in figures 6a, b. Note in particular the strong Coanda effect shown in figure 6b, with the flow adhering to the upper wall expansion and a large separation bubble on the lower wall during the expansion. The wall shear corresponding to figure 6a is plotted in figure 7. We also note the presence of a wave

downstream, with separation bubbles alternating on the two walls. Such a wave is well known in steady channel flow over a backward-facing step (Armaly *et al.* 1983) and is particularly marked for unsteady flow in a non-uniform channel (Sobey 1985; Tutty & Pedley 1993). The last columns of table 4 give the values of $z = \beta e^x$ at which the shear stress is zero on the two walls according to each of the three Navier–Stokes solutions at the Reynolds number 300 ($\delta = 3.0$) and for the two asymmetric solutions at $Re = 500$ ($\delta = 5.0$).

All the Navier–Stokes results presented use 33 points across the channel and 5001 along it. As a check on the accuracy of these results, calculations were performed for $Re = 300$ and 500 with 49 points across the channel or 2501 along it. These confirmed the validity of the flow patterns shown in figures 4 and 6, and that values for the separation points given in table 4 are accurate to at least 0.1. A further set of calculations with $Re = 300$ and 500, $z_0 = 40$, and $x_1 = 3.69$ were performed to check the effects of the downstream conditions on the results. While this has a large effect on the flow downstream, it had little effect on the position of separation: with a 33×5001 grid and $Re = 300$, the separation point was at $z = 9.77$ when the initial separation was on the upper wall and $z = 9.78$ when it was on the lower wall. With $Re = 500$ and $z_0 = 40$, the values were the same as those given in table 4 for $z_0 = 20$. Hence, the downstream conditions will affect the position of the initial separation only if the separation is relatively close to the change in shape of the channel. As expected, the value of β did not affect the position of the initial separation in terms of z: a run with the 33×5000 grid, $Re = 500$, $z_0 = 20$, $\beta = 0.4$, and $x_1 = 3.91$ gave $z_s = 6.11$ on the lower wall, as in table 4.

In addition, calculations were performed for the parabolized Navier–Stokes equations in the same channel. The PNS equations are obtained by dropping the streamwise diffusion terms from both momentum equations, and thus resemble the boundary layer equations but with a cross-stream pressure gradient. They differ from the equations used in § 2 *c* above by including a viscous term in the y-momentum equation. In so far as this is negligible for $\delta \gg 1$, however, the results should agree with those of that section. However, there is still an element of upstream influence due to the elliptic nature of the Poisson equation governing the pressure. In streamfunction-vorticity terms the PNS equations are obtained by dropping the streamwise diffusion term from the vorticity transport equation but not from the Poisson equation relating the streamfunction and vorticity. No results for the PNS equations will be presented as they showed little difference from the Navier–Stokes results already given. However, we note that solutions with the flow following either the upper or the lower wall, as in figure 6*a*, *b*, were obtained, which demonstrates the importance of the cross-stream pressure gradient in generating multiple solution branches.

4. Discussion

It is clear from § 2 *a* that the series method is too cumbersome and contaminated by round-off error to be a useful alternative numerical method for computing separated flows in channels of arbitrary geometry. For the particular geometry represented by equations (1.7) and (1.8), however, § 2 *b* shows that the method is simple to implement and can be used for accurate computation of the wall shear distribution even beyond the separation point. The computed values of wall shear and separation point compare well with those obtained by more conventional numerical methods,

PHILOSOPHICAL TRANSACTIONS OF THE ROYAL SOCIETY A MATHEMATICAL, PHYSICAL & ENGINEERING SCIENCES

using the time-independent boundary-layer or Navier–Stokes equations (table 4). It should be noted that good agreement on the position of the separation point (x_s) is a substantial achievement. Figure 3*b* shows that the series solution agrees very closely with its leading term, the lubrication theory solution, until quite close to separation where the direct sum departs abruptly from the Padé sum. It follows that any solution of the boundary layer equations which marches downstream from Poiseuille flow must calculate departures from Poiseuille flow with extreme accuracy, for otherwise the computation of x_s could be substantially in error.

For flows where more than one solution branch exists, the series method can necessarily find just one, the continuation of the unique low-Reynolds-number branch. The flow described by this branch experiences separation from both channel walls at the same value of x (or slightly different values when the cross-section pressure gradient is included), and is likely to be unstable and experimentally unrealizable. It is surprising that the standard numerical solution of the steady boundary layer equations was also unable to find asymmetric solutions, since the analysis of Borgas & Pedley (1990) demonstrates non-uniqueness of solutions of these equations. Three solution branches were found by numerical solution of the steady Navier–Stokes equations: as iteration proceeded, the solution at first tended towards an approximately symmetric flow, but then moved away and converged onto one of the possible asymmetric flows. Such asymmetry is consistent with experimental observation. The behaviour of the iteration procedure reveals a potential danger for computational fluid dynamicists: if we had used a cruder numerical method, or been satisfied with a less stringent convergence criterion, we might have concluded that the Navier–Stokes equations, too, failed to reveal non-uniqueness and asymmetry of separated flow.

The only experiments available for quantitative comparison with the present results are those of Patterson (1934, 1935) and, as explained in the introduction, his symmetric channel was very nearly the same as our asymmetric exponential channel with $\epsilon = 0.05$. Like us, Patterson (1934) observed symmetrical separation for lower Reynolds numbers, $Re = 19$ and $Re = 34$ (though the flow in the separated eddies was markedly three-dimensional at the lower value; compare Bertram & Pedley (1983)), but asymmetrical separation, from one wall or the other, for $Re = 57$ and $Re = 75$. In his second paper, Patterson (1935) attempted to measured the position of the separation point at $Re = 35$, when the flow was symmetric, for comparison with the predictions of Blasius (1910), based on the two-term direct sum. Patterson found that separation occurred approximately where the slope of one channel wall, $\mathrm{d}\hat{z}/\mathrm{d}\hat{x}$, was given by $Re\,\mathrm{d}\hat{z}/\mathrm{d}\hat{x} \approx 6$. Rescaled according to our coordinate system, this is equivalent to

$$\delta\beta \mathrm{e}^{x_s} \approx 12,$$

where we recall that $\epsilon Re = \delta$; the value of δ in the experiments was 1.75.

The computed results of § 2 *b*, as listed in the first column of table 4, give $\delta\beta\mathrm{e}^{x_s}$ equal to 32.6, 33.6 and 34.5 for $\delta = 1$, 3, 5 respectively, nearly three times larger than the experimental value. Since the various computation methods agree rather closely, the discrepancy must be attributable to departures of the experimental conditions from those assumed here: the necessarily three-dimensional nature of the channel, the small discontinuity of slope at $x = 0$, the difficulty of ensuring an absolutely parallel channel for $x < 0$, etc. Moreover, as we have seen, the position of the separation point (and *a fortiori* of e^{x_s}) is very sensitively dependent on upstream conditions. Lucas (1972) made similar observations in this context.

The work described in this paper was begun in 1986 while N.M.B. was visiting T.J.P. at Cambridge, where O.R.T. was a postdoctoral research associate. The paper was completed while T.J.P. was Professor of Applied Mathematics at the University of Leeds. Financial support from the Indian National Science Academy and the SERC is gratefully acknowledged. Explicit formulae for the functions $g_{n,k}(x)$, $n = 1, 2$ (equation (2.8)); $\phi_{2,1}(\eta)$, $\phi_{2,2}(\eta)$ (equation (2.14)); and $\tilde{\phi}_{2,l}(\eta)$, $l = 1, 5$ (equation (2.21)) can be obtained from the authors on request.

References

Armaly, B. F., Durst, F., Pereira, J. C. F. & Schönung, B. 1983 Experimental and theoretical investigation of backward-facing step flow. *J. Fluid Mech.* **127**, 473–496.

Baker, G. A. 1975 *Essentials of Padé approximants.* Academic Press.

Bertram, C. D. & Pedley, T. J. 1983 Steady and unsteady separation in an approximately two-dimensional indented channel. *J. Fluid Mech.* **130**, 315–345.

Blasius, H. 1910 Laminare Strömung in Kanälen wechselnder Breite. *Z. Math Phys.* 58, 225.

Borgas, M. S. & Pedley, T. J. 1990 Non-uniqueness and bifurcation in annular and planar channel flows. *J. Fluid Mech.* **214**, 229–250.

Durst, F., Pereira, J. C. F. & Tropea, C. 1993 The plane symmetric sudden-expansion flow at low Reynolds numbers. *J. Fluid Mech.* **248**, 567–581.

Fearn, R. M., Mullin, T. & Cliffe, K. A. 1990 Nonlinear flow phenomena in a symmetric sudden expansion. *J. Fluid Mech.* **211**, 595–608.

Fraenkel, L. E. 1962 Laminar flow in symmetrical channels with slightly curved walls. I. On the Jeffery–Hamel solutions for flow between plane walls. *Proc. R. Soc. Lond.* A **267**, 119–138.

Fraenkel, L. E. 1963 Laminar flow in symmetrical channels with slightly curved walls. II. An asymptotic series for the stream function. *Proc. R. Soc. Lond.* A **272**, 406–428.

Graves-Morris, P. R. 1973 *Padé approximants and their applications.* Academic Press.

Gupta, H. 1982 *Selected topics in number theory.* Abacus Press.

Hildebrand, F. B. 1991 *Introduction to numerical analysis.* McGraw-Hill.

Keller, H. B. 1968 *Numerical methods for two-point boundary-value problems.* Blaisdell Press.

Lowan, A. N., Salzer, H. E. & Hillman, A. 1942 A table of coefficients for numerical differentiation. *Bull. Am. Math. Soc.* **48**, 920–924.

Lucas, R. D. 1972 A perturbation solution for viscous incompressible flow in channels. Ph.D. dissertation, Stanford University.

Patterson, G. N. 1934 Flow forms in a channel of small exponential divergence. *Can. J. Res.* **11**, 770–779.

Patterson, G. N. 1935 Viscosity effects in a channel of small exponential divergence. *Can. J. Res.* **12**, 676–685.

Reneau, L. R., Johnston, J. P. & Kline, S. J. 1967 Performance and design of straight, two-dimensional diffusers. *Trans. Am. Soc. Mech. Engrs* D **89**, 141–150.

Sobey, I. J. 1985 Observations of waves during oscillatory channel flow. *J. Fluid Mech.* **151**, 395–426.

Sobey, I. J. & Drazin, P. G. 1986 Bifurcation of two-dimensional channel flows. *J. Fluid Mech.* **171**, 263–287.

Tutty, O. R. & Pedley, T. J. 1993 Oscillatory flow in a stepped channel. *J. Fluid Mech.* **247**, 179–204.

Van Dyke, M. 1975 *Perturbation methods in fluid mechanics*, 2nd edn. Parabolic Press.

Van Dyke, M. 1984 Computer-extended series. *A. Rev. Fluid Mech.* **16**, 287–309.

Ward-Smith, A. J. 1980 *Internal fluid flow.* Oxford: Clarendon Press.

Wilson, S. D. R. 1969 The development of Poiseuille flow. *J. Fluid Mech.* **38**, 793–806.

Received 15 June 1994; revised 29 March 1995; accepted 2 August 1996

PHILOSOPHICAL TRANSACTIONS OF THE ROYAL SOCIETY A MATHEMATICAL, PHYSICAL & ENGINEERING SCIENCES